10-9-2016

Slip Distribution of the 2014 Mw=8.1 Pisagua, Northern Chile, Earthquake Sequence Estimated From Coseismic Fore-Arc Surface Cracks

John P. Loveless
Smith College, jloveles@smith.edu

Chelsea P. Scott
Cornell University

Richard W. Allmendinger
Cornell University

Gabriel González
Universidad Católica del Norte

AGU PUBLICATIONS

Geophysical Research Letters

RESEARCH LETTER
10.1002/2016GL070284

Key Points:
- We estimate coseismic slip of the 2014 Pisagua earthquake sequence using geologic data
- Coseismically generated surface cracks systematically vary in orientation along the coastline
- The slip distributions are consistent with estimates from geodetic and seismic data

Supporting Information:
- Supporting Information S1
- Figure S1
- Figure S2
- Figure S3
- Table S1

Correspondence to:
J. P. Loveless,
jloveless@smith.edu

Citation:
Loveless, J. P., C. P. Scott, R. W. Allmendinger, and G. González (2016), Slip distribution of the 2014 $M_w = 8.1$ Pisagua, northern Chile, earthquake sequence estimated from coseismic fore-arc surface cracks, *Geophys. Res. Lett.*, *43*, 10,134–10,141, doi:10.1002/2016GL070284.

Received 1 JUL 2016
Accepted 14 SEP 2016
Accepted article online 17 SEP 2016
Published online 9 OCT 2016

Slip distribution of the 2014 $M_w = 8.1$ Pisagua, northern Chile, earthquake sequence estimated from coseismic fore-arc surface cracks

John P. Loveless[1], Chelsea P. Scott[2], Richard W. Allmendinger[2], and Gabriel González[3,4]

[1]Department of Geosciences, Smith College, Northampton, Massachusetts, USA, [2]Department of Earth and Atmospheric Sciences, Cornell University, Ithaca, New York, USA, [3]Departamento de Ciencias Geológicas, Universidad Católica del Norte, Antofagasta, Chile, [4]Centro Nacional de Investigación para la Gestión Integrada de Desastres Naturales, Antofagasta, Chile

Abstract The 2014 $M_w = 8.1$ Iquique (Pisagua), Chile, earthquake sequence ruptured a segment of the Nazca-South America subduction zone that last hosted a great earthquake in 1877. The sequence opened >3700 surface cracks in the fore arc of decameter-scale length and millimeter-to centimeter-scale aperture. We use the strikes of measured cracks, inferred to be perpendicular to coseismically applied tension, to estimate the slip distribution of the main shock and largest aftershock. The slip estimates are compatible with those based on seismic, geodetic, and tsunami data, indicating that geologic observations can also place quantitative constraints on rupture properties. The earthquake sequence ruptured between two asperities inferred from a regional-scale distribution of surface cracks, interpreted to represent a modal or most common rupture scenario for the northern Chile subduction zone. We suggest that past events, including the 1877 earthquake, broke the 2014 Pisagua source area together with adjacent sections in a throughgoing rupture.

1. Introduction

Understanding the spatial distribution of coseismic slip is crucial for placing an earthquake in tectonic and societal contexts, as it allows for comparison with records of strong ground motion [*Graves*, 1998], preseismic coupling [*Loveless and Meade*, 2011; *Moreno et al.*, 2010], and the distribution of postseismic processes including the aftershock sequence [*King et al.*, 1994], afterslip on the source fault [*Evans and Meade*, 2012; *Miyazaki et al.*, 2004], and viscoelastic relaxation [*Hearn et al.*, 2002; *Pollitz et al.*, 2000]. The proliferation of local and global seismic and geodetic observing systems has permitted high-resolution estimation of the static and dynamic rupture processes, often in near real time.

We present here the first estimation of a coseismic slip distribution based on field observations of surface deformation features produced by an earthquake sequence, inferring the rupture of the 1 April 2014 $M_w = 8.1$ Pisagua, northern Chile, earthquake and its 3 April $M_w = 7.7$ aftershock from >3700 small-scale cracks breaking the surface of the northern Chile fore arc [*Scott et al.*, 2016]. While mapping the distribution of surface rupture along a source fault has complemented geophysical studies of continental earthquakes such as the 2010 El Mayor, Mexico, [*Gold et al.*, 2013] and 2003 Bam, Iran, [*Fielding et al.*, 2005] events, the coseismic cracks we use as constraining data are located ≥50 km from the rupture zone of the Pisagua earthquake sequence, representing secondary deformation in response to coseismically generated stress changes. Crack orientations vary on a spatial scale similar to the rupture length of the earthquakes in the sequence [*Scott et al.*, 2016] and provide diagnostic information about the patterns of coseismic slip. The fresh cracks opened by the Pisagua earthquake sequence reactivated existing fractures and are similar to long-lived structures throughout the northern Chilean fore arc. The Pisagua cracks provide evidence that a single earthquake is capable of generating permanent deformation in the fore arc. Furthermore, this deformation represents but an increment of the accumulated strain that region-wide cracks record over a nearly million-year time scale [*Baker et al.*, 2013], which we interpret as indicating repeated opening due to a most common or modal rupture pattern of great earthquakes [*Loveless et al.*, 2009]. Thus, the fresh cracks not only provide information about the stresses imposed by the 2014 earthquake sequence but also allow us to interpret this sequence in the context of long-term subduction zone seismicity.

2. Estimated Slip From Coseismic Surface Cracks

The March–April 2014 Pisagua earthquake sequence consisted of a foreshock sequence, $M_w = 8.1$ main shock, and aftershock sequence including the $M_w = 7.7$ event [González et al., 2015], and it represents the first great earthquake along the "Iquique Gap" segment of the Andean subduction zone since 1877. The sequence generated thousands of decameter-scale length, millimeter- to centimeter-scale aperture open cracks in the fore arc. We measured the location and orientation of more than 3700 such fresh surface cracks, the vast majority representing reactivation of preexisting fractures, at 72 localities in the fore arc of northern Chile [Scott et al., 2016]; we did not comprehensively sample the apertures or lengths of these structures. The spatial distribution and orientation of these cracks were documented during field campaigns carried out 2 weeks, 6 weeks, and 3 months after the earthquake sequence. As such, though we refer to cracks as being formed coseismically, we cannot rule out the possibility that cracks represent deformation from the immediate postseismic period. We use the cracks as indicators of coseismically applied tension arising from the slip process on the underlying subduction zone interface. Specifically, we assume that static tension acted in a direction normal to crack strike in order to cause coseismic opening, although locally, cracks display evidence of some oblique opening.

Based on comparison with the orientation of static principal strain axes estimated from coseismic GPS displacement gradients, we selected a subset of crack sites to constrain the slip distribution of the $M_w = 8.1$ main shock. Thirty-one crack populations, representing a total of 1787 individual cracks, are attributed to the main shock based on the similarity between site-averaged strike and trend of the minimum principal extension direction from the geodetic strain analysis, in which principal strain axes are calculated on a grid of 10 km spacing by inverting [Cardozo and Allmendinger, 2009] the GPS data using a 50 km distance weighting factor [Scott et al., 2016]. At 27 sites, cracks show similarity with strain axes calculated from coseismic displacements related to the $M_w = 7.7$ aftershock, which we use to estimate the slip distribution for that event. At 14 sites, cracks have an average strike that differs from both the main shock and the $M_w = 7.7$ aftershock strain axes by $>50°$. Cracks at these sites are subparallel to regional fault scarps, and thus, we attribute their formation as associated with topographic focusing of seismic waves [Scott et al., 2016].

We interpret the angular agreement between the crack strikes and principal strain axes as indication that the same static stress field is responsible for generating geodetically observed coseismic displacements and causing opening of the cracks. We use the strain axis-based selection of crack populations attributed to the main shock and aftershock described above only to discriminate subsets of data used to estimate the slip distribution of these events, but it is important to note that we use neither the geodetic displacements themselves nor the derived strain as formal constraints in the crack-based estimation of slip.

2.1. Estimation Methodology

Linear elastic dislocation theory establishes a first-order relationship between slip on modeled fault surfaces and displacement, strain, and stress throughout homogeneous elastic half-space. We use this theory to describe how slip on the Nazca subduction zone interface, represented using triangular dislocation elements (TDEs) capable of capturing along-strike and downdip geometric complexity as expressed in the U.S. Geological Survey Slab 1.0 model [Hayes et al., 2012], generated static stress changes in the fore arc where coseismic cracks are observed. We calculate the partial derivatives [Meade, 2007] relating unit strike and dip slip on the subduction zone TDEs to the full stress tensor at each crack site then transform each stress tensor into a local coordinate system, with axes (1) parallel to mean crack strike at the site, (2) parallel to dip (vertical), and (3) normal to the mean crack attitude. Each locality is assigned a normal stress magnitude proportional to the spatial density of observed cracks. We use this suite of projected normal stresses to estimate the distribution of subduction interface slip, separately for the main shock and aftershock, subject to Laplacian smoothing to regularize the underdetermined problem [Desbrun et al., 1999], with weighting proportional to the nominal resolving capability of the crack data [Loveless and Meade, 2011] (Figure S3 in the supporting information). Uncertainties on the projected normal stresses are proportional to the standard deviation of the suite of measured crack strikes at each location, under the assumption that cracks with uniform orientation and hence small variance better constrain the direction of applied stress. We use MATLAB's constrained linear least squares optimization and impose constraints on slip in the dip direction to ensure reverse motion and limit strike-slip motion to ±1 m, yielding estimated coseismic slip at a high angle to the subduction trench, consistent with the azimuth of relative plate motion [Angermann et al., 1999].

2.2. Stress Magnitude Scaling

The magnitude of estimated slip is linearly related to the magnitude of stress inferred to have generated the cracks. Spatial variation in this stress magnitude is poorly constrained by the cracks, and as such, we focus on using the spatial distribution of site-averaged crack strikes to constrain the gradient, rather than the absolute magnitude, of coseismic slip. However, to facilitate comparison with independent estimates of the coseismic slip distributions, we uniformly scale the stress magnitude at each crack site so that the estimated slip distribution yields an earthquake of $M_w = 8.1–8.2$ for the main shock and $M_w = 7.6–7.7$ for the aftershock (Figure S1). The uniform scaling factor is determined by taking the median of the crack-perpendicular normal stress magnitudes calculated at all sites using a point source approximation of each earthquake, with parameters based on the event's entry in the Global Centroid Moment Tensor catalog [*Dziewonski et al.*, 1981; *Ekström et al.*, 2012]. We assume that crack density, calculated as number of cracks at a particular site normalized by the maximum distance between the site centroid and the site's individual cracks, is proportional to normal stress magnitude to constrain the rupture area and gradient of coseismic slip, and so we multiply the point source median stress by the crack density value to give the stresses used in the slip inversion (Table S1). We also test inversions using (1) uniform stress at all sites, and stress magnitudes proportional to (2) number of cracks at each site and (3) number of cracks normalized by the site area, and we find similarities among these estimated slip distributions.

Coseismic cracks may be generated by both static and dynamic stress, the latter associated with the passage of seismic waves. Our estimation method for coseismic slip makes the inherent assumption that the static stress is representative of the stress that generated cracks, supported by the agreement between static principal strain axes derived from coseismic GPS displacements and observed crack strikes. While principal stress axis orientations vary through time as seismic waves pass through the fore arc, simulations of dynamic stress for past Andean subduction events [*Loveless et al.*, 2009] suggest that the temporal distribution of principal stress orientation is tightly clustered around the predicted static stress direction. However, the presence of the free surface, near-surface material properties, and topographic focusing of static and dynamic stress, which are not considered here under the assumption of a homogeneous elastic half-space, likely influence stress magnitudes and spatial density of cracks. Both the Pisagua coseismic cracks and longer-lived cracks distributed throughout the northern Chile fore arc represent data sets well suited for future exploration of the roles these rheologic and topographic factors play in generating near-surface deformation.

2.3. Evaluating Goodness-of-Fit

We evaluate the goodness-of-fit of the estimated slip distributions by first calculating the full stress tensor at each constraining crack site as predicted by the estimated slip distribution then comparing the trend of the most compressive principal horizontal stress axis (σ_1) with the site-averaged crack strike. This comparison implies a horizontal σ_3 axis perpendicular to crack strike and hence in the direction of crack opening. The goodness-of-fit varies as a function of how heavily the Laplacian smoothing operator is weighted in the slip estimation (Figure S1). The slip distribution shown in Figure 1a reflects a compromise fit to the crack orientation data and coseismic GPS displacements (Figure S1a), which were not used as formal constraints on the slip estimation. For this main shock model, the average angular error, representing the absolute value of the angle between the mean crack strike and σ_1 trend, across the constraining crack sites is 12.9°, and the angular error at 64% of sites is less than the standard deviation of crack strikes observed at the site. More generally, the observed regional-scale pattern of crack strike variation is mimicked by the principal stress orientations predicted by the model (Figure 1a), with northeast strikes and trends south of the main slip region and northwest orientations to the north. The preferred aftershock slip distribution (Figure 1b) fits the constraining crack strikes with an average angular error of 17.9°, with errors at 48% of sites less than the standard deviation of strikes.

3. Comparing Crack-Based Slip Distribution to Other Estimates

In addition to evaluating the goodness-of-fit of our crack-based coseismic slip estimates to the constraining data, we compare the slip distributions to estimates made from GPS, interferometric synthetic aperture radar, strong motion, teleseismic, and tsunami data [*An et al.*, 2014; *Duputel et al.*, 2015; *Gusman et al.*, 2015; *Hayes et al.*, 2014; *Liu et al.*, 2015; *Schurr et al.*, 2014; *Yagi et al.*, 2014]. For the main shock, the crack-based 2 m slip contour shows spatial overlap that from with other estimates, while the peak slip is located around 70.9°W,

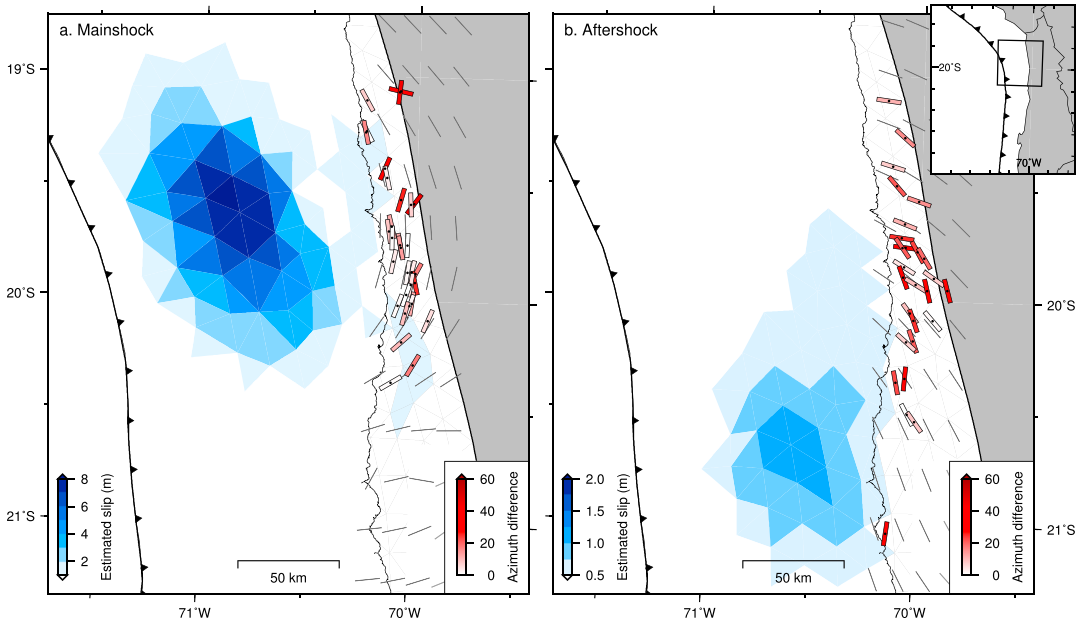

Figure 1. (a) The 1 April 2014 $M_w = 8.1$ Pisagua earthquake main shock slip distribution estimated from coseismic crack orientation data. Triangular dislocation elements representing the subduction interface are colored by estimated slip, equivalent to an earthquake of $M_w = 8.1$. Onshore, bars are oriented parallel to the mean strike of observed coseismic cracks at 31 field sites and are colored by the azimuth difference, defined as the absolute value of the angle between mean observed strike and forward prediction of crack strike at these sites, given as maximum principal compression direction (σ_1). Gray lines show σ_1 axes at gridded locations to illustrate the regional trend in predicted crack strikes. (b) Slip distribution for the 3 April $M_w = 7.7$ aftershock, estimated using the mean strike of observed coseismic cracks at 27 field sites, with symbols as in a. Inset map shows study area and Andean subduction trench. Figure S1 shows the azimuth differences for each event at all 72 sites where coseismic cracks were observed.

19.5°S, northwest of that derived from other data sets (Figure 2a). For the aftershock, we find peak slip occurring south of the main shock, consistent with previous estimates [*Hayes et al.*, 2014; Schurr et al., 2014] (Figure 2a), though the 1 m slip contour and peak slip location are located ~25–50 km south of those of other estimates. Estimation of subduction interface slip from crack orientations is affected by the same geographical bias as that from geodetic data sets: we have no offshore observations directly overlying the region of greatest subduction zone slip (Figure S3).

To formally compare the spatial correlation of the crack-based main shock slip distribution with estimates made from other data sets (specifically, *An et al.* [2014], *Duputel et al.* [2015], *Hayes et al.* [2014], and *Schurr et al.* [2014]), we first interpolate the published slip maps onto our subduction zone geometry and then calculate the correlation coefficient among the slip magnitudes. The crack-based slip distribution shows the strongest spatial correlation (correlation coefficient of 0.80 ± 0.04) with that of *Schurr et al.* [2014] and is, on average, as strongly correlated with alternative slip maps (0.54 ± 0.07) as are *An et al.* [2014] and *Duputel et al.* [2015] (averages of 0.55 ± 0.07 and 0.56 ± 0.07, respectively; Figure 2b). That is, the crack-based slip estimate is as similar to previously published slip distributions estimated from geodetic, seismic, and/or tsunami data as most of these estimates are to each other.

As another means of testing the compatibility between the crack-based slip distribution and other data measuring coseismic deformation, we use our estimated main shock slip to calculate [*Meade*, 2007] predicted coseismic displacements at regional GPS stations. These predicted displacements show generally good agreement with the spatial pattern of observed coseismic motion; our predicted GPS displacements have a mean residual magnitude of 2.4 cm (Figure 3). Displacements predicted by our model are smaller in magnitude than the observations and have azimuths that are, on average between 18°S–22°S, rotated ~15° clockwise from the observed vectors. This is consistent with the location of a concentration of our estimated slip to the northwest of slip distributions constrained by geophysical data, including GPS displacements (Figure 2a).

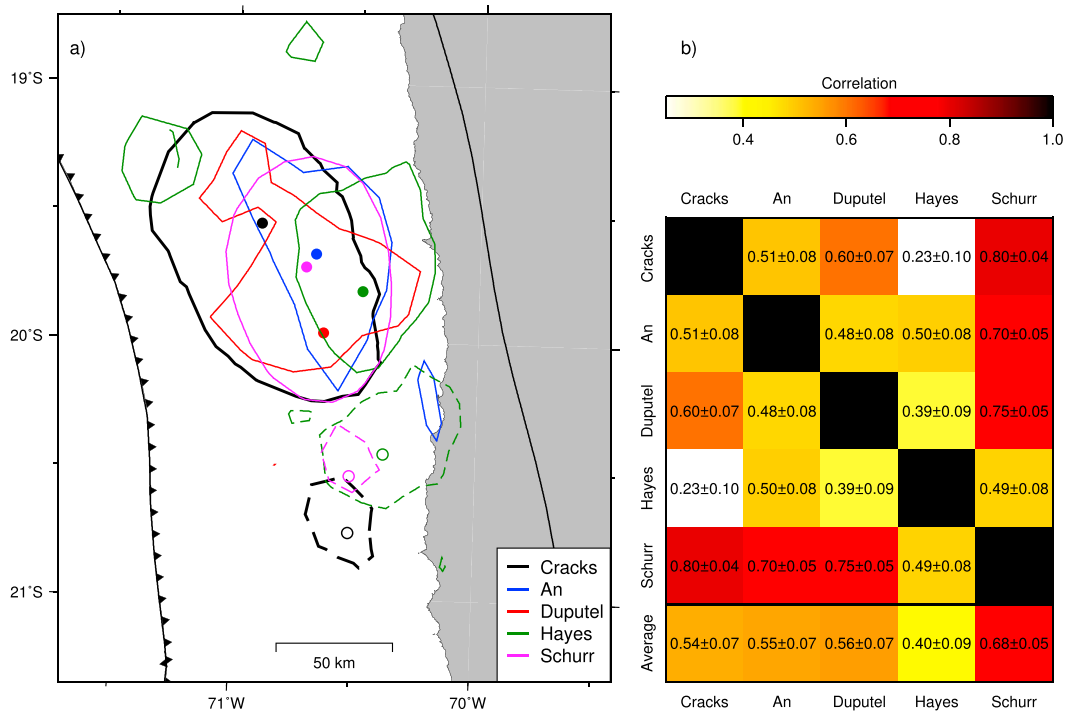

Figure 2. Comparisons of crack-based slip distributions with published estimates. (a) Solid colored lines and filled dots, respectively, show the estimated 2 m slip contour and location of maximum slip from coseismic slip distribution estimates for the 1 April main shock: black, crack based; blue, *An et al.* [2014]; red, *Duputel et al.* [2015]; green, *Hayes et al.* [2014]; and magenta, *Schurr et al.* [2014]. Dashed lines and hollow dots show the 1 m slip contour and peak slip location, respectively, for the 3 April aftershock. (b) Spatial correlation of estimated main shock slip distributions. Each slip estimate was mapped onto the subduction interface geometry used for the crack-based inversion, and the correlation coefficient was calculated between the slip magnitudes. For each slip estimate, the average row reflects correlations with the four other distributions.

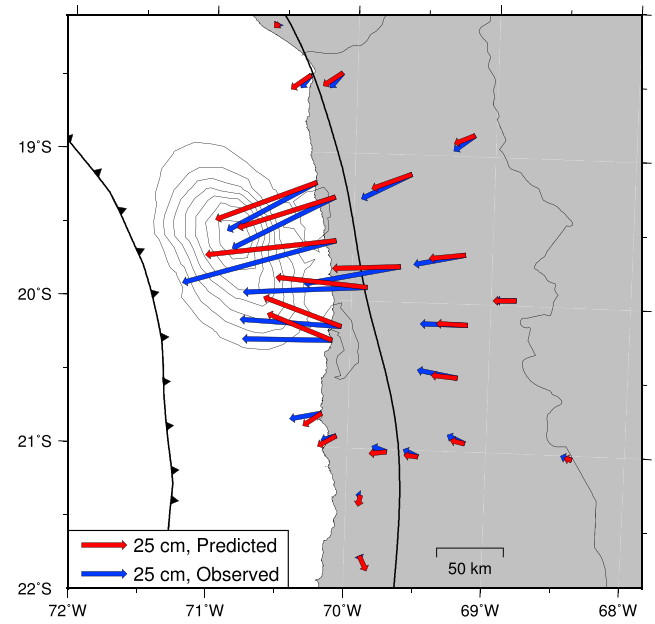

Figure 3. Observed static coseismic GPS displacement vectors (blue) compared to predicted displacements (red) from the crack-based main shock slip estimate (shown as 1 m contours). The GPS vectors were not used as formal constraints in the crack-based slip estimate.

Though the crack strike data could be combined with geodetic observations in a joint inversion for coseismic slip, we choose to present here only the crack-based estimates. Using the cracks alone highlights an independent means of estimating slip from geologic data. While the crack data may provide unique information to a joint inversion, the nonuniqueness involved in weighting multiple data sets in such an inversion may cloud the relationship between slip and permanent deformation that we present in this paper.

4. Relationship Between Fresh and Existing Cracks

Many cracks formed during the Pisagua earthquake sequence are within existing weathered cracks,

having exploited weaknesses already present in the crust [*Scott et al.*, 2016] that were likely generated by thousands of past earthquakes [*Baker et al.*, 2013; *Loveless et al.*, 2009]. Nonetheless, the consistency between the static stress directions predicted by our geologically constrained inversion for the 2014 Pisagua events and those constrained by geodetic, seismic, and tsunami observations, reflecting the similarity in the estimated slip distributions (Figure 2), indicates that the Pisagua earthquake sequence produced stress capable of reopening existing cracks. That is, even if preexisting cracks were oriented oblique to the coseismically induced stress, the Pisagua event must have imposed sufficient coseismic tension normal to crack strikes to cause opening of fresh fissures. While field evidence of lateral offset suggests some nonorthogonal opening of Pisagua earthquake cracks [*Scott et al.*, 2016], the relative proportion of shear and opening is unknown, and so we assume that tensile stresses dominated crack reactivation. The misfit between observed mean crack strikes and predicted static σ_1 axes (Figure 1) therefore inherently reflects both model prediction error as well as our assumption that the cracks truly are mode 1 fractures. The systematic clockwise rotation of our predicted GPS vectors relative to the observations (Figure 3) may suggest that the strikes of measured cracks are not aligned with the true coseismically imposed σ_1 directions: if the actual coseismic stress field arose from a slip distribution more consistent with the GPS data than that constrained by the crack strikes, fresh cracking must have included a component of shearing in addition to opening.

5. Implications for Past and Future Iquique Gap Earthquakes

More than 50,000 measured surface cracks similar to those attributed to the 2014 Pisagua earthquake sequence are present in northern Chile and southernmost Peru [*Baker et al.*, 2013; *Keefer and Moseley*, 2004; *Loveless et al.*, 2009, 2005], which we have interpreted as geologic records of accumulated damage due to thousands of subduction zone earthquakes [*Loveless et al.*, 2009] over 100 kyr time scales [*Baker et al.*, 2013]. We hereinafter refer to these as "imagery-mapped cracks," as we have documented the majority of them with high-resolution satellite imagery, with field-based ground-truthing of select sites revealing that some cracks penetrate tens of meters into bedrock.

We use our estimated Pisagua main shock slip distribution to calculate the predicted principal stress directions at the imagery-mapped crack sites for comparison with the observed strikes [*Loveless et al.*, 2009]. The average azimuth difference between the predicted σ_1 axes and observed site-averaged crack strikes is 54.6° (Figure 4b), suggesting that the strikes of any individual imagery-mapped cracks reopened by the 2014 earthquake deviate substantially from the mean strike at these sites. In other words, only the most favorably oriented subset of imagery-mapped cracks was reactivated. The obliquity between observed orientations and our predicted stress field may also suggest that imagery-mapped cracks could have been affected by tensile stress to cause the opening, as well as crack-parallel shear stress.

Using a similar methodology to this study, we estimated a long-term slip distribution using the imagery-mapped crack strikes [*Loveless et al.*, 2009] that can be interpreted as a modal slip distribution, reflecting the most common slip pattern that would induce stresses capable of repeatedly opening the observed cracks (Figure 4). The imagery-mapped cracks reflect episodes of repeated opening, documented by observations of vertically laminated salt deposits on bedrock crack walls [*Loveless et al.*, 2009]. Under the assumptions that cracks are reactivated by coseismically imposed stresses and that the cracks most favorably aligned with the most frequently imposed principal tension axes will have an obvious surface expression evident in satellite imagery, we interpret the slip distribution estimated based on imagery-mapped crack strikes [*Loveless et al.*, 2009] to represent the most common, or modal, slip pattern on the northernmost Chile segment of the subduction zone.

We focus on the area north of 22°S latitude, where the spatial density of imagery-mapped crack populations resolves better the modal coseismic slip than to the south, though strong interseismic coupling inferred from geodetic observations between 22° and 24°S [*Bejar-Pizarro et al.*, 2013; *Métois et al.*, 2013; *Schurr et al.*, 2014] hints at impending great earthquakes along that segment as well. Modal slip is spatially consistent with estimated interseismic coupling [*Schurr et al.*, 2014] north of ~21°S, with the along-strike extent of a concentration of coupling similar to that of large magnitude modal slip (Figure 4a). This agreement suggests that the future earthquake hazard implied by strong coupling is similar to a great earthquake slip pattern estimated from the imagery-mapped cracks, which reflect the accumulated fore-arc deformation from thousands of plate boundary events.

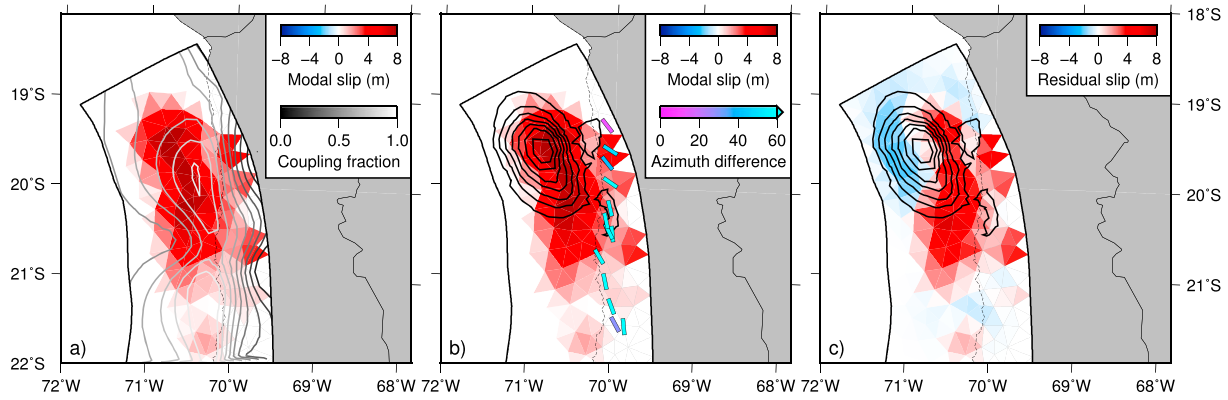

Figure 4. Comparison of interseismic coupling, modal slip, and 2014 earthquake slip. (a) Colored triangles show long-term modal slip distribution estimated from imagery-mapped crack orientations [*Loveless et al.*, 2009] overlain with contours of interseismic coupling estimated from geodetic observations [*Schurr et al.*, 2014]. The contour interval is 0.1 of the plate convergence rate. (b) Modal slip distribution overlain by 1 m contours showing crack-based estimated 2014 Pisagua main shock slip distribution. Onshore, bars show regionally distributed, long-term, imagery-mapped crack strikes, colored by the azimuth difference between site-averaged strike and the σ_1 direction predicted by our 2014 Pisagua main shock slip distribution. (c) Long-term modal slip distribution with 2014 slip subtracted, suggesting adjacent yet unruptured asperities.

Subtracting our estimated slip distribution of the 2014 Pisagua earthquake from the modal slip distribution provides an interpretation of remaining earthquake potential on the northernmost Chile segment of the subduction zone (Figure 4c). As in the case of the Pisagua earthquake, there is uncertainty in the magnitude of slip estimated from the regional-scale distribution of cracks; *Loveless et al.* [2009] scaled the estimated modal slip distribution to a maximum of 8 m to yield a moment magnitude consistent with historical estimates of Iquique Gap events ($M \sim 8.5$–9.0) [e.g., *Comte and Pardo*, 1991]. Under that assumption, we find that the Pisagua earthquake locally mimics the proposed longer-term pattern (Figure 4c) but leaves open the possibility of future great earthquakes to the south of the 2014 source region, consistent with the suggestion of *Hayes et al.* [2014]. The rupture area of the 2014 earthquake sequence is smaller than that estimated for the 1877, but proposed epicenters and magnitudes of other historical earthquakes, including the 1615 (70.5°W, 19.5°S, $M \sim 7.9$), 1833 (71.0°W, 19.0°S, $M \sim 7.4$), and 1869 (70.2°W, 19.6°S, $M \sim 7.4$) events [*Comte and Pardo*, 1991], are more consistent with rupture of a smaller portion of the northern Chile subduction interface as occurred in 2014. In terms of future potential hazard, the close temporal spacing of the 1833 and 1869 earthquakes with the giant 1877 event suggests the possibility that an 1877-like rupture may occur in the coming decades despite—or perhaps associated with—the moment released in the 2014 Pisagua sequence.

Acknowledgments

We gratefully acknowledge National Science Foundation RAPID Award 1443410 (to R.W.A.) and the Centro Nacional de Investigación para la Gestión Integrada de Desastres Naturales (CIGIDEN; grant CONICYT/FONDAP 15110017 to G.G.) of Chile for supporting the fieldwork that documented surface cracks. Scott was supported by the McMullen Fellowship from Cornell University, New York. All crack location and strike observations are published as a data repository item accompanying *Scott et al.* [2014]. We thank William Barnhart for helpful discussions and Zacharie Duputel and Bernd Schurr for providing numerical versions of the published slip and coupling distributions shown in Figures 2 and 4. Romain Jolivet and an anonymous referee provided careful reviews that improved the manuscript and inspire our future work on this topic.

References

An, C., I. Sepúlveda, and P. L.-F. Liu (2014), Tsunami source and its validation of the 2014 Iquique, Chile, earthquake, *Geophys. Res. Lett.*, *41*, 3988–3994, doi:10.1002/2014GL060567.

Angermann, D., J. Klotz, and C. Reigber (1999), Space-geodetic estimation of the Nazca-South America Euler vector, *Earth Planet. Sci. Lett.*, *171*, 329–334.

Baker, A., R. W. Allmendinger, L. A. Owen, and J. A. Rech (2013), Permanent deformation caused by subduction earthquakes in northern Chile, *Nat. Geosci.*, *6*(6), 492–496, doi:10.1038/Ngeo1789.

Bejar-Pizarro, M., A. Socquet, R. Armijo, D. Carrizo, J. Genrich, and M. Simons (2013), Andean structural control on interseismic coupling in the North Chile subduction zone, *Nat. Geosci.*, *6*(6), 462–467, doi:10.1038/Ngeo1802.

Cardozo, N., and R. W. Allmendinger (2009), SSPX: A program to compute strain from displacement/velocity data, *Comput. Geosci.*, *35*(6), 1343–1357, doi:10.1016/j.cageo.2008.05.008.

Comte, D., and M. Pardo (1991), Reappraisal of great historical earthquakes in the northern Chile and southern Peru seismic gaps, *Nat. Hazards*, *4*(1), 23–44, doi:10.1007/BF00126557.

Desbrun, M., M. Meyer, P. Schröder, and A. H. Barr (1999), Implicit fairing of irregular meshes using diffusion and curvature flow, in *Proceedings of the 26th Annual Conference on Computer Graphics and Interactive Techniques, edited*, pp. 317–324, ACM Press/Addison-Wesley Publishing Co., New York.

Duputel, Z., et al. (2015), The Iquique earthquake sequence of April 2014: Bayesian modeling accounting for prediction uncertainty, *Geophys. Res. Lett.*, *42*, 7949–7957, doi:10.1002/2015GL065402.

Dziewonski, A. M., T.-A. Chou, and J. H. Woodhouse (1981), Determination of earthquake source parameters from waveform data for studies of global and regional seismicity, *J. Geophys. Res.*, *86*, 2825–2852, doi:10.1029/JB086iB04p02825.

Ekström, G., M. Nettles, and A. M. Dziewonski (2012), The global CMT project 2004–2010: Centroid-moment tensors for 13,017 earthquakes, *Phys. Earth Planet. Inter.*, *200–201*, 1–9, doi:10.1016/j.pepi.2012.04.002.

Evans, E. L., and B. J. Meade (2012), Geodetic imaging of coseismic slip and postseismic afterslip: Sparsity promoting methods applied to the great Tohoku earthquake, *Geophys. Res. Lett.*, *39*, L11314, doi:10.1029/2012GL051990.

Fielding, E. J., M. Talebian, P. A. Rosen, H. Nazari, J. A. Jackson, M. Ghorashi, and R. Walker (2005), Surface rupture and building damage of the 2003 Bam, Iran earthquake mapped by satellite synthetic aperture radar interferometric correlation, *J. Geophys. Res.*, *110*, B03302, doi:10.1029/2004JB003299.

Gold, P. O., M. E. Oskin, A. J. Elliott, A. Hinojosa-Corona, M. H. Taylor, O. Kreylos, and E. Cowgill (2013), Coseismic slip variation assessed from terrestrial lidar scans of the El Mayor–Cucapah surface rupture, *Earth Planet. Sci. Lett.*, *366*, 151–162, doi:10.1016/j.epsl.2013.01.040.

González, G., P. Salazar, J. P. Loveless, R. W. Allmendinger, F. Aron, and M. Shrivastava (2015), Upper plate reverse fault reactivation and the unclamping of the megathrust during the 2014 Northern Chile earthquake sequence, *Geology*, *43*(8), 671–674, doi:10.1130/G36703.1.

Graves, R. W. (1998), Three-dimensional finite-difference modeling of the San Andreas fault: Source parameterization and ground-motion levels, *Bull. Seis. Soc. Am.*, *88*(4), 881–897.

Gusman, A. R., S. Murotani, K. Satake, M. Heidarzadeh, E. Gunawan, S. Watada, and B. Schurr (2015), Fault slip distribution of the 2014 Iquique, Chile, earthquake estimated from ocean-wide tsunami waveforms and GPS data, *Geophys. Res. Lett.*, *42*, 1053–1060, doi:10.1002/2014GL062604.

Hayes, G. P., D. J. Wald, and R. L. Johnson (2012), Slab1.0: A three-dimensional model of global subduction zone geometries, *J. Geophys. Res.*, *117*, B01302, doi:10.1029/2011JB008524.

Hayes, G. P., M. W. Herman, W. D. Barnhart, K. P. Furlong, S. Riquelme, H. M. Benz, E. Bergman, S. Barrientos, P. S. Earle, and S. Samsonov (2014), Continuing megathrust earthquake potential in Chile after the 2014 Iquique earthquake, *Nature*, *512*(7514), 295–298, doi:10.1038/Nature13677.

Hearn, E. H., R. Burgmann, and R. E. Reilinger (2002), Dynamics of Izmit earthquake postseismic deformation and loading of the Duzce earthquake hypocenter, *Bull. Seis. Soc. Am.*, *92*(1), 172–193.

Keefer, D. K., and M. E. Moseley (2004), Southern Peru desert shattered by the great 2001 earthquake: Implications for paleoseismic and paleo-El Niño–Southern Oscillation records, *Proc. Natl. Acad. Sci. U.S.A.*, *101*, 10,878–10,883, doi:10.1073/pnas.0404320101.

King, G. C. P., R. S. Stein, and J. Lin (1994), Static stress changes and the triggering of earthquakes, *Bull. Seis. Soc. Am.*, *84*(3), 935–953.

Liu, C., Y. Zheng, R. Wang, and X. Xiong (2015), Kinematic rupture process of the 2014 Chile M_w 8.1 earthquake constrained by strong-motion, GPS static offsets and teleseismic data, *Geophys. J. Int.*, *202*(2), 1137–1145, doi:10.1093/gji/ggv214.

Loveless, J. P., and B. J. Meade (2011), Spatial correlation of interseismic coupling and coseismic rupture extent of the 2011 $M_w = 9.0$ Tohoku-oki earthquake, *Geophys. Res. Lett.*, *38*, L17306, doi:10.1029/2011GL048561.

Loveless, J. P., G. D. Hoke, R. W. Allmendinger, G. González, B. L. Isacks, and D. A. Carrizo (2005), Pervasive cracking of the northern Chilean Coastal Cordillera: New evidence for forearc extension, *Geology*, *33*(12), 973–976, doi:10.1130/G22004.1.

Loveless, J. P., R. W. Allmendinger, M. E. Pritchard, J. L. Garroway, and G. Gonzalez (2009), Surface cracks record long-term seismic segmentation of the Andean margin, *Geology*, *37*(1), 23–26, doi:10.1130/G25170a.1.

Meade, B. J. (2007), Algorithms for the calculation of exact displacements, strains, and stresses for triangular dislocation elements in a uniform elastic half space, *Comput. Geosci.*, *33*, 1064–1075, doi:10.1016/j.cageo.2006.12.003.

Métois, M., A. Socquet, C. Vigny, D. Carrizo, S. Peyrat, A. Delorme, E. Maureira, M. C. Valderas-Bermejo, and I. Ortega (2013), Revisiting the North Chile seismic gap segmentation using GPS-derived interseismic coupling, *Geophys. J. Int.*, *194*(3), 1283–1294, doi:10.1093/Gji/Ggt183.

Miyazaki, S., P. Segall, J. Fukuda, and T. Kato (2004), Space time distribution of afterslip following the 2003 Tokachi-oki earthquake: Implications for variations in fault zone frictional properties, *Geophys. Res. Lett.*, *31*, L06623, doi:10.1029/2003GL019410.

Moreno, M., M. Rosenau, and O. Oncken (2010), 2010 Maule earthquake slip correlates with pre-seismic locking of Andean subduction zone, *Nature*, *467*, 198–202, doi:10.1038/nature09349.

Pollitz, F. F., G. Peltzer, and R. Bürgmann (2000), Mobility of continental mantle: Evidence from postseismic geodetic observations following the 1992 Landers earthquake, *J. Geophys. Res.*, *105*, 8035–8054, doi:10.1029/1999JB900380.

Schurr, B., et al. (2014), Gradual unlocking of plate boundary controlled initiation of the 2014 Iquique earthquake, *Nature*, *512*(7514), 299–302, doi:10.1038/nature13681.

Scott, C. P., R. W. Allmendinger, G. González, and J. P. Loveless (2016), Coseismic extension from surface cracks reopened by the 2014 Pisagua, Northern Chile earthquake sequence, *Geology*, *44*(5), 387–390, doi:10.1130/G37662.1.

Yagi, Y., R. Okuwaki, B. Enescu, S. Hirano, Y. Yamagami, S. Endo, and T. Komoro (2014), Rupture process of the 2014 Iquique Chile earthquake in relation with the foreshock activity, *Geophys. Res. Lett.*, *41*, 4201–4206, doi:10.1002/2014GL060274.